AEDC-TR-79-92

Electro-Optical Pressure-Measurement Techniques

H. T. Bentley III and P. J. Murphy
ARO, Inc.

May 1980

Final Report for Period October 1, 1978 – September 30, 1979

Approved for public release; distribution unlimited

ARNOLD ENGINEERING DEVELOPMENT CENTER
ARNOLD AIR FORCE STATION, TENNESSEE
AIR FORCE SYSTEMS COMMAND
UNITED STATES AIR FORCE

NOTICES

When U. S. Government drawings, specifications, or other data are used for any purpose other than a definitely related Government procurement operation, the Government thereby incurs no responsibility nor any obligation whatsoever, and the fact that the Government may have formulated, furnished, or in any way supplied the said drawings, specifications, or other data, is not to be regarded by implication or otherwise, or in any manner licensing the holder or any other person or corporation, or conveying any rights or permission to manufacture, use, or sell any patented invention that may in any way be related thereto.

Qualified users may obtain copies of this report from the Defense Technical Information Center.

References to named commerical products in this report are not to be considered in any sense as an indorsement of the product by the United States Air Force or the Government.

This report has been reviewed by the Office of Public Affairs (PA) and is releasable to the National Technical Information Service (NTIS). At NTIS, it will be available to the general public, including foreign nations.

APPROVAL STATEMENT

This report has been reviewed and approved.

Marshall K. Kingery

MARSHALL K. KINGERY
Project Manager
Directorate of Technology

Approved for publication:

FOR THE COMMANDER

Marion L. Laster

MARION L. LASTER
Director of Technology
Deputy for Operations

REPORT DOCUMENTATION PAGE		READ INSTRUCTIONS BEFORE COMPLETING FORM
1 REPORT NUMBER AEDC-TR-79-92	2 GOVT ACCESSION NO.	3 RECIPIENT'S CATALOG NUMBER
4 TITLE (and Subtitle) ELECTRO-OPTICAL PRESSURE-MEASUREMENT TECHNIQUES		5 TYPE OF REPORT & PERIOD COVERED Final Report - October 1, 1978 to September 30, 1979 6 PERFORMING ORG REPORT NUMBER
7 AUTHOR(s) H. T. Bentley III and P. J. Murphy, ARO, Inc., a Sverdrup Corporation Company		8 CONTRACT OR GRANT NUMBER(s)
9 PERFORMING ORGANIZATION NAME AND ADDRESS Arnold Engineering Development Center/DOT Air Force Systems Command Arnold Air Force Station, Tennessee 37389		10 PROGRAM ELEMENT, PROJECT, TASK AREA & WORK UNIT NUMBERS Program Element 65807F
11 CONTROLLING OFFICE NAME AND ADDRESS Arnold Engineering Development Center/DOS Air Force Systems Command Arnold Air Force Station, Tennessee 37389		12 REPORT DATE May 1980 13 NUMBER OF PAGES 37
14 MONITORING AGENCY NAME & ADDRESS(if different from Controlling Office)		15 SECURITY CLASS (of this report) UNCLASSIFIED 15a DECLASSIFICATION DOWNGRADING SCHEDULE N/A

16 DISTRIBUTION STATEMENT (of this Report)

Approved for public release; distribution unlimited.

17 DISTRIBUTION STATEMENT (of the abstract entered in Block 20, if different from Report)

18 SUPPLEMENTARY NOTES

Available in Defense Technical Information Center (DTIC)

19 KEY WORDS (Continue on reverse side if necessary and identify by block number)

electrooptics
pressure measurement
optical membranes
pressure distribution
test methods
wind tunnels

20 ABSTRACT (Continue on reverse side if necessary and identify by block number)

An investigation of the potential application of electro-optical techniques for the measurement of surface pressure distributions was conducted, and several candidate methods were reviewed. The most promising technique utilizes the optical and mechanical properties of a reflective circular membrane. The characteristics of an ideal membrane are analyzed with respect to membrane tension, static pressure, and dynamic membrane response.

DD FORM 1 JAN 73 1473 EDITION OF 1 NOV 65 IS OBSOLETE

20. ABSTRACT (Continued)

Expressions to approximate the yield and bursting pressures of a circular membrane are also presented. Two different automated data acquisition systems were developed. The first relied on measurement of reflected image light intensity, and the second measured the image area to infer applied pressure. The automated systems yielded comparable results, which were in excellent agreement with conventional semiconductor pressure transducer measurements. The use of optical membranes as pressure transducers was found to have several possible limitations, including the effects of model strain and temperature. However, none of these limitations appears so severe as to preclude the use of the method in situations for which it would clearly be more advantageous than conventional methods.

AFSC
Arnold AFS Tenn

PREFACE

The work reported herein was conducted by the Arnold Engineering Development Center (AEDC), Air Force Systems Command (AFSC). The results were obtained by ARO, Inc., AEDC Division (a Sverdrup Corporation Company), operating contractor for the AEDC, AFSC, Arnold Air Force Station, Tennessee, under ARO Project Numbers B35I-P5A, P35I-P5, and P35L-01A (B35L-01A). The manuscript was submitted for publication on October 24, 1979.

CONTENTS

ILLUSTRATIONS

Figure Page

TABLES

1.0 INTRODUCTION

For design and testing of aircraft and missile systems and components, accurate and detailed knowledge of the surface pressure distribution is required yet difficult to obtain for some testing applications. The measurement of surface pressure distributions using electro-optical techniques offers several significant advantages in comparison to conventionally obtained pressure measurements. Some of these potential advantages are

1. simultaneous, time-resolved, multiple pressure distribution measurements,
2. the elimination of bulky and complex wiring and hardware,
3. very high frequency response,
4. reduced model preparation expense and installation time,
5. increased model rigidity for certain configurations, and
6. reduction of boundary-layer flow disturbances.

One such technique entails optical detection of the pressure-induced response of a membrane fabricated into a model surface. Using optical membranes as pressure transducers is neither new nor innovative; however, advances in electro-optical technology permit the economical integration of systems that both complement and supplement conventional pressure-measurement technology in wind-tunnel application. Therefore, the objective of the work reported herein was to evaluate the present feasibility of applying electro-optical techniques to pressure measurement. Several techniques were examined; the advantages and limitations of each were identified. The optical membrane approach was identified as that most promising for tunnel testing applications; this approach is detailed, including the following aspects: the theory of optical membranes as optical elements, deformation dependence on tension, yield strength, dynamic response, and non-ideal effects such as temperature. Some aerodynamic considerations are given for the experimental data-reduction techniques which are discussed. This report provides the basic analytical framework required for evaluating the applicability of the technique.

2.0 REVIEW OF OPTICAL TECHNIQUES

A survey of optical phenomena suitable for surface pressure measurement was conducted. The investigation was limited to those phenomena that require passive devices whose implementation requires minimal model modification. Polarization, absorption spectra, physical shape, transmittance, reflectance, and complex index of refraction are a

few of the identifiable optical characteristics of materials that are pressure dependent. Many of these properties require high applied pressures to be accurate. Other phenomena were not investigated because of their incompatability with test unit environments.

Five candidate techniques are discussed, including (1) pressure dependence of reflectivity in selenium, (2) birefringence effect in optical materials, (3) interferometric measurement of pressure induced thickness variation in materials, (4) liquid crystals, and (5) optical membranes.

2.1 REFLECTIVITY IN SELENIUM

Several optical phenomena sensitive to pressure are briefly outlined. Most of the phenomena occurring in gases and liquids were deemed unsuitable, and only a few of the phenomena occurring in solids were considered.

The pressure dependence of reflectivity for both trigonal and amorphous selenium has been measured between 1.1 and 4.5 eV (Ref. 1). In the case of crystalline selenium, a polarization-dependent shift in the reflectance peak toward lower energy with applied pressure occurs at the rate of $(4.0 \pm 0.3) \times 10^{-5}$ eV/bar. Between 1 and 2 eV, a corresponding fractional change of reflectivity with pressure was noted, 4.4×10^{-5}/bar at peak sensitivity. It is unfortunate that the accuracy required of reflectance measurements greatly exceeds present measurement capabilities, and attempting to obtain such accurate measurements would be complicated further by surface contamination present in many AEDC tunnels.

2.2 STRESS BIREFRINGENCE

Stress birefringence using the mechanical and optical properties of high polymers [such as polymethylmethacrylate (PMMA) and polycarbonate of bisphenol A (PCBA)] has been a useful tool for studying planar stresses (Ref. 2). Optical retardation is proportional to the principal stresses in the media. Almost all transparent materials—including glass, synthetic resins, and plastic—exhibit some degree of double refraction. For planar objects within the elastic limit, the difference between the two principal stresses can be optically measured:

$$\sigma_1 - \sigma_2 = \frac{t_c n}{s}$$

where $\sigma_1 - \sigma_2$ is the difference between principal stresses, s is the thickness, f_σ is the fringe constant of the material, and n is the fringe order. Aside from the obvious problem of transforming normal forces into planar forces, the technique is limited in resolution for solids (f_σ typically ranges from 1 to 1,000 psi/in.-order). Using polarization sensing techniques and assuming a resolution of 1/20 of a fringe order for a thickness of 0.125 in., an optimum resolution of 0.5 psi would be possible. A pressure-measuring technique based on this principle seems only marginally acceptable.

2.3 INTERFEROMETRIC THICKNESS MEASUREMENT

A similar technique was proposed that used interferometric methods to monitor pressure-induced thickness variations in plastics. For a material thickness of 0.125 in., a sensitivity of approximately 1 psi was predicted. This was verified experimentally with use of Plexiglas® as the active material. Helium-neon (He-Ne) laser beam reflections from the front and back surfaces of the material produce observable interference fringes. The intensity variation attributable to fringe motion was monitored and related to the applied pressure. It is unfortunate that most materials are strongly temperature-dependent, rendering them unacceptable for this application. Another problem is posed by the required critical optical alignment.

2.4 LIQUID CRYSTALS

The use of liquid crystal properties has also been proposed. However, in the liquid state, the crystals reorient after application of a stress, thus making a technique based on liquid crystal optical polarization properties valid only for transient pressures. Liquid crystals are also sensitive to temperature. Thus, further investigation was not deemed productive.

2.5 MEMBRANE AS AN OPTICAL TRANSDUCER

Of all five methods identified, the use of optical membranes appears to be the most promising. The use of deformable membranes as optical transducers is not without precedent, although the application to wind tunnels has been limited to special cases of low-speed, turbulent boundary-layer flow.

During the early 1940's the optical system of the Golay cell was developed by the U. S. Army Signal Corps engineering labs as a pneumatic infrared transducer. The instrument has been used frequently in the fields of infrared physics and astronomy. The device, an extension of the Hayes cell (Ref. 3), was first modified by Zahl to provide an interferometric readout (Ref. 4). The final version of the Golay cell (Ref. 5) embodied a deformable optical membrane. The optical system consists of a gas-filled radiation-receiving chamber with a

heat-absorbing membrane at one end. Infrared radiation incident on the receiving cell causes expansion of the gas in the chamber. The membrane is distended, acting as a spherical mirror. Outside the cell, light from the source passes through a line grid and is reflected by the membrane surface, which re-images the line grid onto a second similar grid. Variations in the membrane curvature produce a shifting of the grid image. A photodetector monitors the light level variation.

More recently, Budal described an optical microphone (Ref. 6). In this application, a metal-coated Mylar® membrane again serves as the sensing element. A light source and a balanced pair of photodetectors are used to cancel noise. Frequency response to 20 kHz has been reported over a dynamic range from 44 db(c) to 131 db(c) with less than 6-percent distortion. The operating principle is similar to that of the Golay cell in that the grid imaging technique is used.

A membrane mirror assembly with electrostatic actuators has been used as an optimum device for introducing phase corrections to an aberrated wave (Refs. 7 and 8). The devices use relatively large-area membranes, up to 125 mm^2, that are as thin as 0.25 μm. Membranes have been manufactured from titanium, titanium alloys, nickel, beryllium, and molybdenum. The titanium membranes are produced by evaporating the material onto a substrate in vacuum.

A pressure-measuring technique was developed by Bentley and Belz in 1972, using a deformable membrane as the pressure-sensing element. The focal position of each sensor was determined by holographically recording a wave reflected from the membrane surface. Reconstruction of the hologram at a later time was required to recover the data. The data retrieval time, in addition to the precision required by the holographic process, limits general application of the technique.

The most promising of the membrane transducer applications was for investigating the instantaneous structure of the wall pressure distribution under a turbulent boundary layer (Refs. 9, 10, and 11). The method required a Michelson interferometer in which one mirror was replaced by a reflecting, flexible wall. Data were recorded with a high-speed camera for later analysis. The flexible wall consisted of a thin silicone rubber foil approximately 35 μm thick, overcoated with aluminum and stretched across a rigid base containing 650 drilled holes. Data reduction required detailed interpretation of fringe motion, together with a pretest calibration. Analysis of the interferometric data was both time consuming and difficult. Considerable effort was expended in reducing tunnel vibrations and other noise because of the nature of the interferometric technique. The approach provided heretofore

unattainable data such as the instantaneous wall pressure distribution, in addition to the convection velocity and the wall pressure gradient.

3.0 MEMBRANE PRESSURE TRANSDUCER THEORY

The optical pressure-measuring systems proposed herein all require an optical membrane pressure transducer. The device consists of a small circular aperture covered by a relatively thin, elastic membrane. An analytical framework will be developed relating the membrane's geometric properties and, hence, its optical properties, to optical geometry, material properties, and pressure-temperature environment. For the ideal membrane theory development, it shall be assumed that (1) the membrane is clamped around its circumference, (2) the film thickness is small, compared to the aperture radius, and (3) displacements are on the order of the film thickness. The third assumption is necessary only for vibration analysis and constant tension assumptions. The generalized theory allows for variations in tension caused by deformation and thermal expansion.

3.1 IDEALIZED MEMBRANE THEORY

When acted upon by a differential pressure, an elastic, reflective, circular membrane forms a surface suitable for use as an optical pressure transducer (OPT). A brief analysis of the optical and physical properties follows.

The optical pressure transducer acts as a variable-focal-length element, shown in the equivalent optical system in Fig. 1. A point source illuminates the OPT over a circular area of radius a about its optical axis. If it is assumed that the OPT acts as a spherical focusing element of focal length f, then the distance to the image point is given by the lens equation:

$$Z_f = \left(\frac{1}{f} - \frac{1}{Z_s}\right)^{-1} \tag{1}$$

where Z_s is the distance of the point source in front of the optical pressure transducer.

In the observation plane, the image radius is given by

$$\iota(Z_i) = \rho\left(\frac{Z}{Z_f} - 1\right) \tag{2}$$

$$= \rho\left[Z\left(\frac{1}{f} - \frac{1}{Z_s}\right) - 1\right] \tag{3}$$

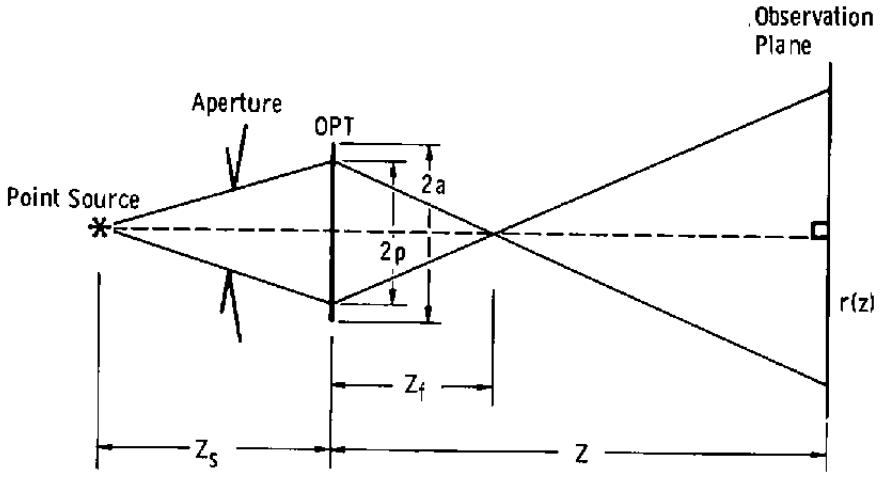

Figure 1. Equivalent optical system.

where Z is the distance between the undeflected transducer surface and the plane of observation and ϱ is the aperture radius. A distinction between the membrane radius, a, and the illuminated radius, ϱ, is made.

The OPT focal length is related to the radius of curvature, R_c, by

$$f = \frac{R_c}{2} \tag{4}$$

for a spherical mirror element. The radius of curvature, R_c, is designated positive if the surface is deflected inward. This also serves to define a positive pressure differential (Fig. 2).

An expression for radius of curvature is obtained from a force balance around the transducer periphery. The normal forces attributable to pressure must be balanced by the normal forces at the boundary caused by tension (see Fig. 2):

$$R_c = \frac{2T}{P} \tag{5}$$

where T is the tension in the membrane and P is the pressure differential. In general, the tension is not constant; it varies with temperature, material properties, and amount of deflection. Equation (5) is exact for uniform, isotropic tension which leads to spherical deformation. The validity of this relationship holds for any infinitesimally small area.

Substituting Eq. (5) into Eq. (3), together with Eq. (4), yields the following relationship between the pressure and the image radius of the observation plane:

$$r(Z) = \rho\left[Z\left(\frac{P}{T}-\frac{1}{Z_c}\right)-1\right] \tag{6}$$

For constant tension, a linear relationship between image size and pressure would be expected. However, tension is only constant for a zero pressure differential. The assumption of constant tension in Eqs. (5) and (6) is valid only for high initial tension or for membrane deflections that are on the order of the membrane thickness. In either of these cases, the pressure sensitivity of the membrane is drastically reduced.

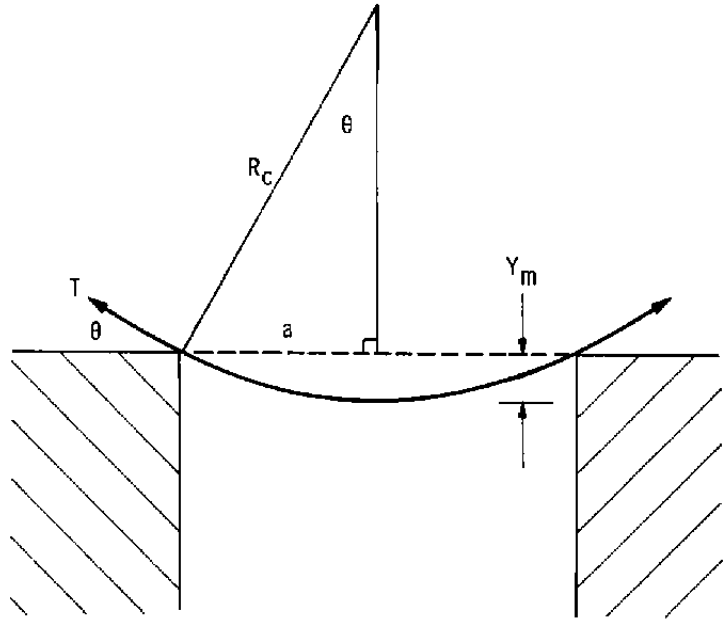

Figure 2. Optical membrane geometry.

3.2 GENERALIZED TENSION THEORY

To account for tension changes caused by strain, one must examine the changes in strain from all sources. These include the effects of membrane deflection and temperature dependent expansion

The area strain, ϵ_A, is related to the linear strain by

$$\epsilon_A = \frac{dA}{A} = \epsilon_x + \epsilon_y + 2\epsilon_x\epsilon_y \simeq 2\epsilon \tag{7}$$

where ϵ_x and ϵ_y are the components of the membrane-surface linear strain, which is induced by area change on deformation. If an isotropic membrane is assumed, then $\epsilon_x = \epsilon_y = \epsilon$.

The three linear components of strain are interrelated (Fig. 3) (Ref. 12):

$$\epsilon_x = \frac{1}{E}\left[\sigma_x - \mu(\sigma_y + \sigma_z)\right] + \alpha\Delta t$$

$$\epsilon_y = \frac{1}{E}\left[\sigma_y - \mu(\sigma_x - \sigma_z)\right] + \alpha\Delta t \tag{8}$$

$$\epsilon_z = \frac{1}{E}\left[\sigma_z - \mu(\sigma_x + \sigma_y)\right] + \alpha\Delta t$$

where E is the elastic modulus of the material and μ is Poisson's ratio. The effects of temperature are included in the $\alpha\Delta t$ term where α is the coefficient of thermal expansion and Δt is the temperature change. The surface tension is defined in terms of the stress for thin membranes as $T = \sigma\delta$ where $\sigma_x = \sigma_y = \sigma$, and δ is the membrane thickness. Since $\sigma_z = P << \sigma$, the strain equations reduce to

$$T = \frac{E\delta(\epsilon - \alpha\Delta t)}{(1-\mu)} + T_o \tag{9}$$

The total strain is the result of two effects: (1) the initial strain in the undeformed membrane, which results in a tension, T_o, and (2) the additional strain produced by the area change during deformation given by ϵ. ϵ_A can be determined by referring to Fig. 3.

The maximum displacement, Y_m, is given by the solution to the following quadratic equation:

$$Y_m^2 - 2R_c Y_m + a^2 = 0 \tag{10}$$

After expansion in a binomial series, the solution becomes

$$Y_m = \frac{a^2}{2R_c} + \frac{a^4}{8R_c^3} + \cdots \tag{11}$$

The area strain, however, is given by

$$\epsilon_A = \frac{A_f - A_i}{A_i} \tag{12}$$

or

$$\epsilon_A = \frac{2R_c Y_m}{a} - 1 \tag{13}$$

where A_f and A_i are, respectively, the final and initial areas.

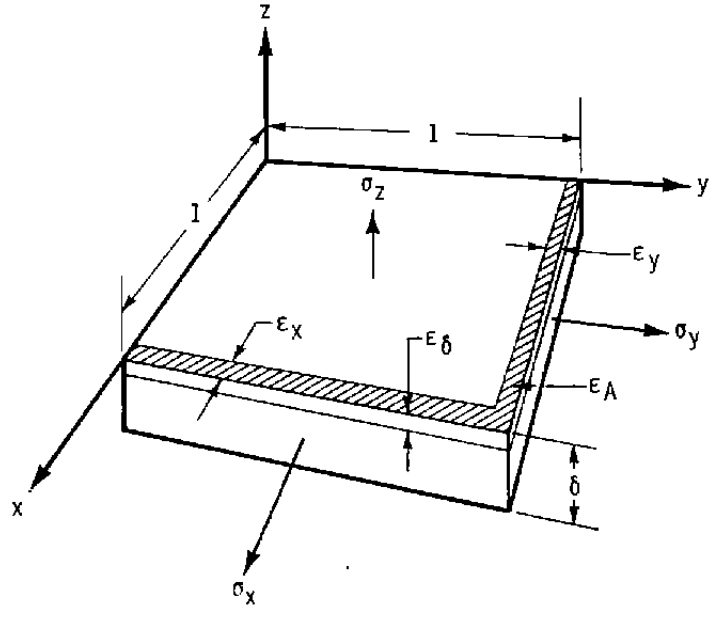

Figure 3. Strain in a thin membrane.

Substituting Eq. (11) into Eq. (13) yields

$$\epsilon_A = \frac{1}{4}\left(\frac{a}{R_c}\right)^2 \tag{14}$$

After the relationship for the radius of curvature is substituted, Eq. (14) becomes

$$\epsilon_A = \frac{P^2 a^2}{16\Gamma^2} \tag{15}$$

The expression for the net tension in the membrane is then given by

$$\Gamma = \frac{E\delta\left(\frac{P^2 a^2}{16\Gamma^2} - 2\alpha\Delta t\right)}{2(1-\mu)} + T_o \tag{16}$$

Eqs. (6) and (15) can be combined to yield a generalized relationship for pressure in terms of measurable optical quantities and material properties. This is given by

$$P = \psi\left[\frac{E\delta a^2 \psi^2}{32(1-\mu)} - \frac{E\delta\alpha\Delta t}{(1-\mu)} + T_o\right] \tag{17}$$

where ψ is defined as the linear function of image radius

$$\psi \equiv \frac{1}{Z}\left(\frac{r}{\rho} + \frac{Z}{Z_s} + 1\right) \tag{18}$$

Again, the distinction is made between the membrane radius, a, and the illuminated radius, ϱ, because some form of aperturing may be used. Note that Eq. (17) allows for pressure calculation with no knowledge of membrane tension other than T_o. This seemingly complicated relationship can be put into the form

$$P = A\psi^3 + T_{eff}\psi \tag{19}$$

where

$$A = \frac{E\delta a^2}{32(1-\mu)}$$

and

$$T_{eff} = T_o - \frac{E\delta\alpha\Delta t}{(1-\mu)} \tag{20}$$

It is now evident that P becomes a linear function of ψ (hence r) for T_o sufficiently large and for small values of ψ. The effective equivalency of temperature and initial tension is also evident. Increasing the temperature of a membrane with a positive coefficient of expansion (note that some thermoplastics have a negative coefficient) reduces the effective tension, T_{eff} (see Fig. 4). Consequently, the sensitivity to pressure change is increased. It is also possible for thermal effects to offset completely the initial tension. This is particularly important for wind-tunnel applications above room temperature requiring the construction of transducers with sufficiently high initial tension. The value of α in Eq. (17) represents the difference between the coefficients of thermal expansion of the support structure and the membrane for uniform heating.

Increasing tension results in an increased linear region about P = 0, with a correspondingly reduced sensitivity, $\Delta r/\Delta P$. At higher pressures (which result in higher

tensions) the ψ^3 term dominates and sensitivity becomes independent of temperature and tension and depends only on material properties.

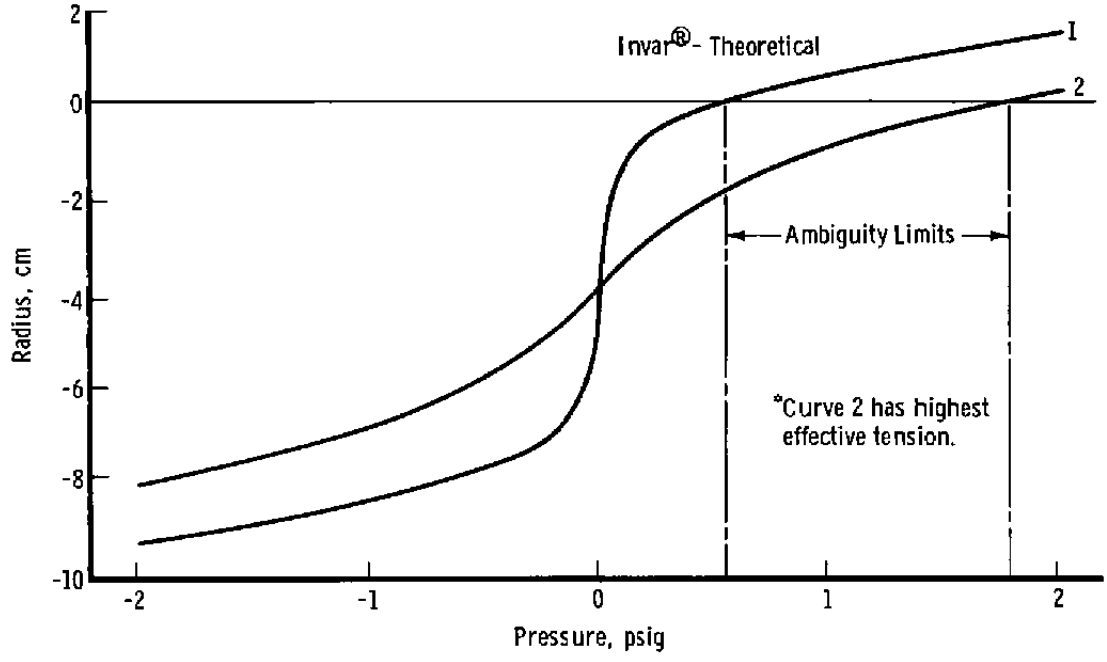

Figure 4. Effects of varying membrane tension.

Another important feature illustrated in Fig. 4 is the ability to shift the ambiguity limit by the selection of a finite prefocal distance, Z_s. The limit is that value of pressure which, by geometric optics, produces a vanishingly small image radius. Since the techniques proposed cannot discriminate between positive and negative images without prior information, this point represents a limit, approachable from either direction, to unambiguous pressure readings. The term Z/Z_s contained in ψ acts as a linear offset to r/ϱ. However, the selection of a finite Z_s, as opposed to planar illumination (where $Z_s \Rightarrow \infty$), requires this additional information for data analysis.

A valid point of concern about the application of optical transducers is the deleterious effect of temperature. The effect can be reduced (1) by applying sufficiently high initial tension or (2) by making suitable pressure calibration by varying the referenced pressure at the equilibrium temperature. The latter approach can be employed at run conditions if the average pressure is being obtained.

3.3 DYNAMIC MEMBRANE RESPONSE

The differential equation for a thin membrane with damping in the presence of a uniform fluctuation pressure field is given by

$$\rho_s \delta \frac{\partial^2 Y}{\partial t^2} + \frac{\beta \partial \overline{Y}}{\partial t} - T\nabla^2 Y = P_a e^{i\omega t} \tag{21}$$

where T is the membrane displacement at any point. The damping term is given as a function of the damping factor, β, and the average displacement over the membrane area:

$$\overline{Y}_m = \frac{1}{2\pi a^2} \int_o^{2\pi} \int_o^a Y r dr d\phi \tag{22}$$

When damping is the result of laminar airflow in a dissipative medium, this assumption appears valid (Ref. 9).

Exact solution of the equation requires detailed knowledge of the transducer and its acoustic environment. An alternate approach will be taken to illustrate some basic properties of the membrane transducer.

3.4 VIBRATION OF AN UNDAMPED MEMBRANE

The differential equation becomes, after neglecting damping and considering free vibration,

$$\nabla^2 Y = \frac{\rho_s \delta}{T} \frac{\partial^2 Y}{\partial t^2} \tag{23}$$

Upon the usual separation of variables and applying the boundary conditions Y = a at r = a, and Y must be everywhere finite and single valued, the general solution is of the form

$$Y(r, \theta, t) = \sum_{m=0}^{\infty} \sum_{n=0}^{\infty} J_{mn}\left(\frac{\omega_{mn} t}{\Gamma}\right) \left[\left(a_{mn} \operatorname{Cos} m\theta + b_{mn} \operatorname{Sin} m\theta \right) \left(\operatorname{Cos} \omega_{mn} t + c_{mn} \operatorname{Cos} m\theta + d_{mn} \operatorname{Sin} m\theta \right) \operatorname{Sin} \omega_{mn} t \right] \tag{24}$$

where

$$\Gamma \equiv \sqrt{\frac{T}{\rho_s \delta}}$$

The material density is given by ρ_s.

The constants can be determined from the additional boundary conditions at t = 0:

$$Y(r, \theta, 0) = f_1(r, \theta) \tag{25}$$

$$\frac{\partial Y}{\partial t}(r, \theta, 0) = f_2(r, \theta) \tag{26}$$

The condition Y (a, θ, t) requires

$$J_m\left(\frac{\omega_{mn} a}{\Gamma}\right) = 0 (m = 1,2,3\ldots) \tag{27}$$

If B_{mn} are the zeroes of the mth order Bessel function, then

$$\omega_{mn} = \frac{\beta_{mn}\Gamma}{a} \tag{28}$$

The fundamental mode, ω_{o_1}, is the lowest natural frequency of the membrane and represents an approximate upper limit to flat transducer response. For pressure fluctuations well below this limit, the membrane can be considered to be compliant, and the previous static results can be applied. The numerical value for the frequency can be computed as

$$f_o = \frac{\omega_{o_1}}{2\pi} = \frac{0.3827}{a}\sqrt{\frac{T}{\rho_s \delta}} \tag{29}$$

The membrane deflection can then be written (Ref. 6)

$$Y = \frac{Pa^2}{4T}\left(1 - \frac{r^2}{a^2}\right)$$

$$= \left(\frac{B_{01}}{4\pi}\right)\frac{P}{\rho_s \delta f_o^2}\left(1 - \frac{r^2}{a^2}\right) \tag{30}$$

This reduces to $Y_m = Pa^2/4T$, which can be obtained from Eqs. (5) and (11). For an example of comparative sensitivities, two transducers are considered in Table 1, one of Mylar and one of brass.

Table 1. Comparative Sensitivities, Mylar® and Brass Transducers

Material	a, cm	T, $\frac{dyne}{cm}$	ρ_s, $\frac{gm}{cm^3}$	δ, cm	f, kHz	Sensitivity, $\frac{cm - cm^2}{dyne}$	Sensitivity, $\frac{in.}{psi}$
Mylar®	0.3175	11×10^5	1.38	2.54×10^{-3}	6.4	$2.5^2 \times 10^{-1}$	6.8×10^{-3}
Brass	0.15875	7.7×10^5	7.8	1.25×10^{-3}	67.8	8.18×10^{-10}	2.22×10^{-5}

The sensitivity is the maximum displacement for a unit of applied pressure. The basic characteristics of a high-frequency response OPT are small size, high tension, and low mass. The trade-off is made in reduced sensitivity. This problem will now be examined in relation to typical sound pressure readings.

3.5 SOUND PRESSURE RESPONSE

The sound pressure level at a given frequency is related to the amount of deformation for a compliant membrane vibrating in its fundamental mode. Sound level in decibels is defined as

$$S[db] \equiv 20 \log_{10}\left(\frac{P}{P_o}\right) \tag{31}$$

where

$$P_o = 0.0002 \frac{dyne}{cm^2}$$

In terms of intensity, the definition becomes

$$S[db] \equiv 10 \log_{10}\left(\frac{I}{I_o}\right) \tag{32}$$

where

$$I_o = 10^{-16} \frac{watt}{cm^2} .$$

The peak sound pressure becomes

$$P_{P_{eak}} = 10^{S/20} P_o \times 1.404$$

when the pressure is defined as the rms value.

For example, 120 db = 280 dyne/cm^2 corresponds to a maximum displacement of 7.0 x 10^{-5}cm for the Mylar transducer, and 2.3 x 10^{-7}cm for the brass transducer. This corresponds to 1.1 x 10^{-3} λ and 3.6 x 10^{-3} λ for He-Ne laser radiation (0.6328 μm), respectively. The Mylar 0.25-in.-diam transducer is within the region of interferometric displacement measurements. Measurement to within 0.25 λ has been demonstrated with a fringe counting system (Refs. 13 and 14). Resolutions to within 0.01 λ have been reported using phase measurement techniques (Ref. 15). An interferometer system in the differential mode, measuring the central membrane deflection, would be useful for a variety of acoustic studies.

3.6 YIELD AND BURSTING PRESSURES

In determining the required membrane properties for specific environmental applications, the bursting pressure of the membrane must be considered. The maximum pressure that a membrane can withstand can be estimated from measurable material properties. Bursting will occur when the stress is approximately equal to the ultimate strength, σ_N, of the membrane material. Tension in the membrane takes the following form:

$$T = \frac{\epsilon E \delta}{(1-\mu)} = \frac{\sigma_N \delta}{(1-\mu)} \tag{33}$$

where the modulus of elasticity, E, is defined as the ratio of stress to strain:

$$E = \frac{\sigma}{\epsilon} \tag{34}$$

The strain for a circular membrane as a function of pressure and tension is

$$\epsilon = \frac{P^2 a^2}{32 T^2} \tag{35}$$

Substituting this value into Eq. (33) and solving for pressure give

$$P_B = \frac{\delta}{a(1-\mu)} \left(\frac{32 \sigma_N^3}{E} \right)^{1/2} \tag{36}$$

This equation gives an approximate value of the bursting pressure, based on material properties.

The stress-strain relationships become nonlinear beyond the elastic limit of the material. The elastic modulus is defined as a proportionality constant only in the linear region of the stress-strain curves. Calculations of bursting pressure are in agreement with experimental data in sources treating shock tube theory (Ref. 16). The actual bursting pressure for metal films nearly always exceeds the theoretical limit predicted above. Possible exceptions to this rule occur for a few plastics, such as Mylar.

Although knowledge of the bursting pressure is required, even more important is the ability to calculate the membrane yield pressure, the pressure that, if exceeded, causes the material to undergo a permanent elastic deformation. This point of permanent deformation under a load is known as the elastic limit. The quantity that is a measure of the stress induced on the membrane at the elastic limit is the yield strength, σ_s. Replacing the tensile strength in Eq. (36) with the yield strength, one can now define the yield pressure as

$$P_Y = \frac{\delta}{a(1-\mu)} \left(\frac{32\ \sigma_s^3}{E} \right)^{1/2} \tag{37}$$

Examples of theoretical calculations of bursting and yield pressures, as compared to experimental data compiled by Gaydon and Hurle, are presented in Table 2 (Ref. 16). This table shows the comparative accuracies of the approximations for several metals and plastics. Table 3 gives several important material properties used in these calculations. Gaydon and Hurle reported that the experimental data are about 10 percent low, a fact that the authors attribute to thinning of the membrane material before rupture. That the error for the plastic materials is higher may be caused by the greater elasticity of the plastics.

4.0 EXPERIMENTAL TECHNIQUES

Experimental verification of the basic optical properties and the corresponding pressure equations served also to demonstrate three possible measurement systems. Each technique measured one of the characteristics associated with the reflected image—the image radius, area, and intensity. The expression ψ used in the pressure equation can be written

$$\psi(r) = \frac{1}{Z} \left(1 + \frac{r}{\rho} - \frac{Z}{Z_s} \right) \tag{38}$$

as before. Measurements of the normalized image radius, r/ϱ, as a function of pressure can be used to verify the pressure equation. ψ can be written in terms of the image area, A, as

$$\psi(A) = \frac{1}{Z} \left(1 \mp \frac{\sqrt{A/\pi}}{\rho} + \frac{Z}{Z_s} \right) \tag{39}$$

Table 2. Bursting and Yield Pressures for Various Membrane Materials*

Material	Thickness, in.	Radius, in.	P_B, Experimental**, psi	P_B, Theory, psi	P_Y, Theory, psi
Mylar®	0.001	1.5	20	33.5	20.5
	0.002	1.5	47	67.0	40.9
	0.0075	1.5	127	251.3	153.5
Cellophane	0.001	0.5	22	---	---
Polyethylene	0.002	1.5	47	11.2	7.3
Copper	0.0075	0.63	500	495.6	224.1
	0.010	0.63	800	660.9	298.7
	0.016	0.63	1300	1057.3	478.0
	0.023	0.63	1900	1516.8	687.1
	0.027	0.63	2400	1784.1	806.6
Aluminum	0.0015	1.25	23	26.6	13.9
	0.004	1.25	65	70.5	37.1
	0.006	1.25	102	105.8	55.4
	0.032	1.6	400	440.3	230.7
	0.064	1.6	800	880.5	461.6
Steel	0.07	8.75	3000	640	256

*Based on constants listed in Table 3.

**Experimental results from Ref. 16, p. 91.

Table 3. Material Properties

Material	$\alpha(c^{-1})$	E, psi	μ	σ_R, psi	σ_S, psi	Density, g/cm^3
Mylar®	30×10^{-6}	0.55×10^6	0.3 to 0.4	25×10^3	8.0×10^3	1.395
TFL Teflon®	100×10^{-6}	0.58×10^6	0.35	3×10^3	---	2.15
Polyethylene	150×10^{-6}	0.10×10^6	0.46	4×10^3	3.0×10^3	0.94
Brass	18.9×10^{-6}	15×10^6	0.34	$*64 \times 10^3$	$*44.0 \times 10^3$	8.47
Aluminum	25.2×10^{-6}	10×10^6	0.33 to 0.35	$*40 \times 10^3$	$*26.0 \times 10^3$	2.70
Copper	16.6×10^{-6}	17×10^6	0.34 to 0.36	$*73 \times 10^3$	$*43.0 \times 10^3$	8.96
Invar®	1.0×10^{-6}	21.4×10^6	0.3	- - -	---	7.75 to 8.0
St. Steel	17.3×10^{-6}	28×10^6	0.3	83 to 145×10^3	76×10^3	8.02
Tin	20.0×10^{-6}	6×10^6	0.33	$*7.10 \times 10^3$	$*3.50 \times 10^3$	7.31
Tungsten	4.5×10^{-6}	52×10^6	0.35	430.0×10^3	---	19.3

*Based on average values for several alloys from CRC Handbook of Tables for Applied Engineering Science, pp. 103-115 (Ref. 17).

where the sign is chosen based on the previously established image radius conventions.

A third alternative for pressure measurement involves the monitoring of image intensity. The total power of a Gaussian laser beam is constant (assuming negligible scattering or attenuation losses). A Gaussian beam always propagates everywhere as a Gaussian, even when imaged by a lens or an OPT. Futhermore, geometric optics predict beam intensities when in the far field of a beam waist (Fig. 5).

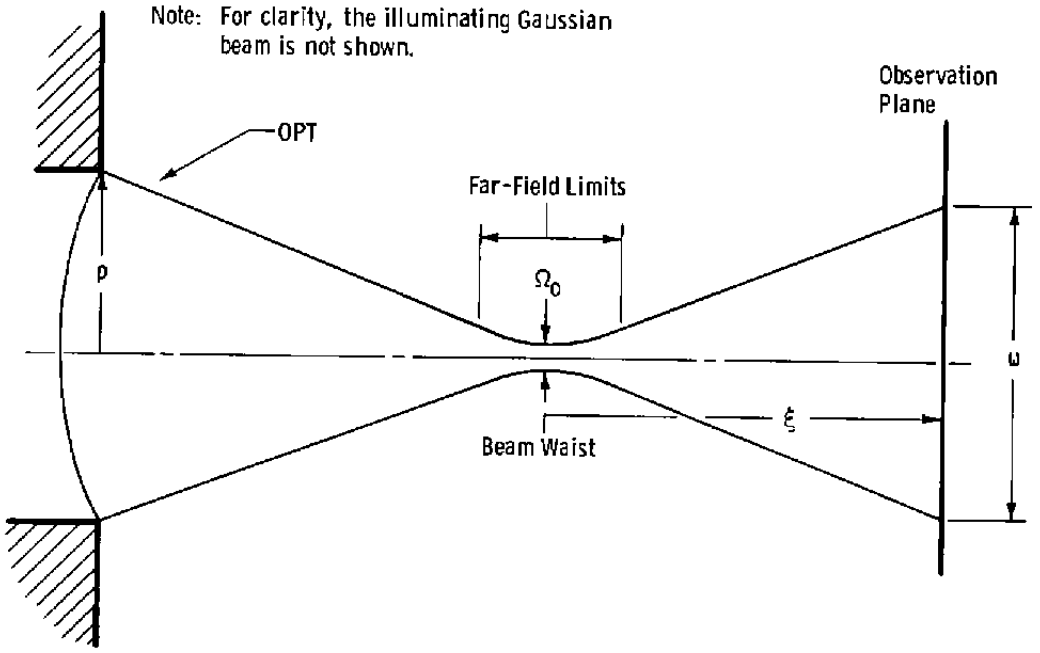

Figure 5. Gaussian beam propagation at geometric limit.

The beam intensity is given by

$$I = I_o e^{-(2r^2/\Omega^2)} \tag{40}$$

where I is intensity and r is the radial distance from the beam axis. The beam diameter, Ω, is defined as the radius at which the intensity is $1/e^2$ or 0.135 of the peak, on axis intensity. The beam diameter can be written

$$\Omega = \Omega_o \left[1 + \left(\frac{\lambda \xi}{\pi \Omega_o^2} \right)^2 \right]^{1/2} \tag{41}$$

where Ω_0 is the beam waist radius at the $1/e^2$ point and ξ is the axial distance from the waist. For $\xi >> \Omega_0^2\pi/2$, the far-field criterion, Ω becomes a linear function of ξ:

$$\Omega \simeq \frac{\lambda\xi}{\pi\Omega_0} \tag{42}$$

ψ can be written in terms of the centerline intensity I at the observation plane and I_p at the OPT center as

$$\psi = \frac{1}{Z}\left(1 \pm \sqrt{\frac{I_p}{I}} + \frac{Z}{Z_s}\right) \tag{43}$$

4.1 IMAGE RADIUS MEASUREMENT

The first experiment was designed to demonstrate the relation between image radius and induced pressure. The apparatus for this experiment consisted of three essential elements: a laser, the pressure transducer, and an imaging screen as shown in Fig. 6. The laser was a standard He-Ne laser operating at a power of 1 mw and a wavelength of 6328 Å. The beam was expanded to 1-in. diameter with a collimator. A diaphragm was placed in the beam path to vary the aperture size for different test runs.

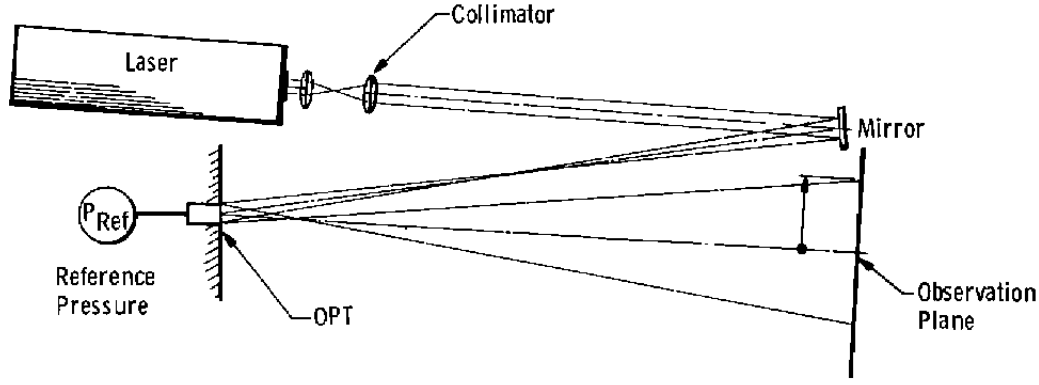

Figure 6. Direct observation of image radius.

Several different transducers were constructed with Mylar Monokote® plastic membranes that had clear apertures ranging from 1/8-in to 1-5/8-in. in diameter, and all had a film thickness of approximately 0.002 in. In addition, a pellicle beamsplitter was mounted to an airtight frame and was used as another pressure transducer. The pellicle transducer had a clear aperture of 1.0 in. and a membrane thickness of 0.000276 in. It was

constructed from a nitrocellulose film. The transducers were each, in turn, connected to a reference pressure cell that supplied the pressure differential to the membranes. The pressure cell was monitored with a conventional electronic pressure transducer with a 1-v/psi sensitivity and a range from 0 to 5 psig. The reference pressure could be read to an accuracy of 0.001 v from a digital voltmeter.

Positive pressures were regulated to the reference cell by creating a slight vacuum inside the pressure cell and transducer cavity and, thereby, producing a concave mirror. Negative pressures were applied by increasing the internal pressure. Most tests performed in the negative pressure range were limited to about -1 psi for the Monokote membranes and to -0.08 psi for the nitrocellulose membrane because the optical membranes were not constructed with tightly clamped edges.

The incident beam illumination was directed onto the membrane surface; an image was formed on a screen about one meter from the center of the transducer. Plane wave illumination was used so that the source distance, Z_s, was located at infinity, and the quantity ψ was reduced to the form of Eq. (38) with Z/Z_s equal to zero. To reduce the need for geometrical corrections and to eliminate aberrations caused by off-axis illumination, experimentation was generally restricted to the paraxial region of the optics. Whenever possible, the beam diameter was restricted to about half the transducer diameter to minimize edge distortion. Simultaneous with the application of a pressure to the membrane, measurements of each radius data point were made by measuring the radius of the image on the screen. The occasional drifting in the zero point of the reference transducer had to be accounted for, but no major problems were encountered.

The radius-pressure data points were plotted with a curve-fitting computer program to determine the values of A and T_{eff} in Eq. (19). This program allowed accurate determination of these constants for each membrane without knowing the precise material properties. The values of A and T_{eff} obtained here were used in the next two phases of experimentation and allowed the utilization of automated data acquisition equipment. The results of two typical test runs are shown in Fig. 7 along with the computer-generated least-squares error curve fit for the 1-5/8-in.-diam Monokote membrane. Several different beam diameters were normalized and used in the construction of this graph. Figure 7 also shows the results obtained with the pellicle transducer. Note by comparison the pressure ranges of the different transducers. The percent-of-range error for both of these membranes was typically less than 2 percent for this measurement technique. The variation in the reference pressure is on the order of ± 0.002 psi, whereas the variation in r/ϱ is ± 0.1 psi.

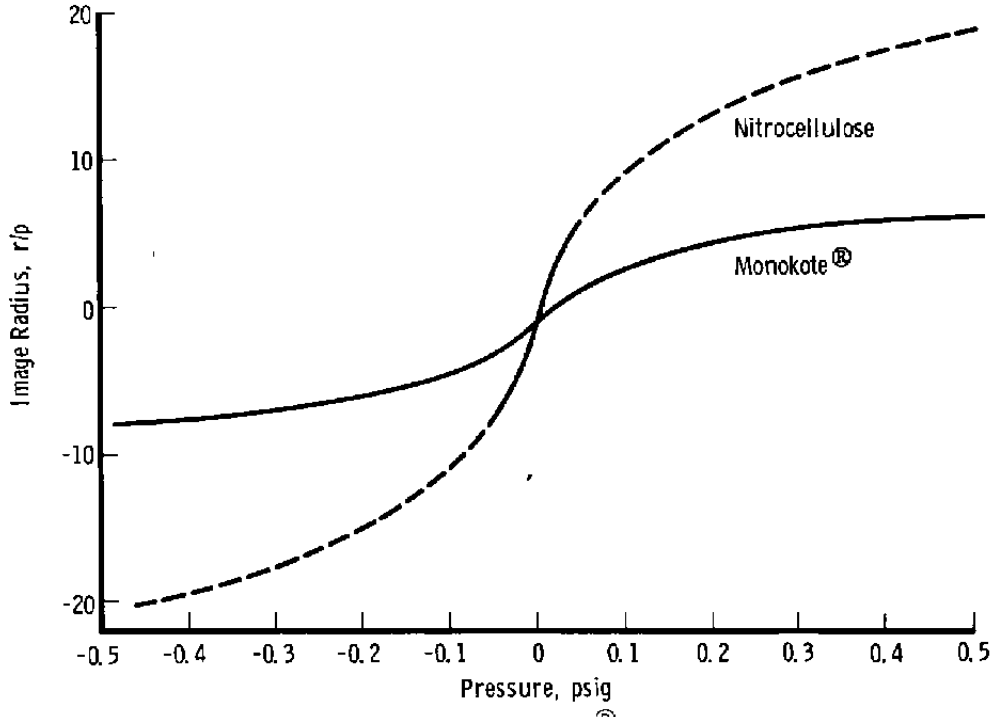

Figure 7. Comparative sensitivity of Monokote® and nitrocellulose membranes.

4.2 INTENSITY MEASUREMENT SYSTEM

The apparatus for the intensity measurement system consisted of two photodetectors to monitor the incident beam and image intensity, plus the equipment mentioned previously. A chopper, operating at 669 Hz, was placed in the beam path to eliminate noise. Each photodetector was referenced to the chopper with separate lock-in amplifiers.

A prototype automatic data acquisition system was used. A Tektronix® 4051 computer was used to program and take data from a Hewlett-Packard 3437A system voltmeter. Through a multiplexer unit, output signals from the reference transducer and the photodetector amplifiers could be sequentially read by the voltmeter and input to the 4051 computer for calculating the pressures and comparing against the measured reference pressure.

The intensity ratio system was calibrated by measuring the image intensity and the reference intensity at $P = 0$. For an aberration-free system, these quantities should be equal, allowing for differences in sensitivities of the amplifiers. The image intensity at $P = 0$, I_o, and the image intensity during the test run, I_i, were normalized to the laser intensity. ψ becomes

$$\psi = \frac{1}{\gamma}\left(1 + \frac{Z}{Z_s} + \sqrt{\frac{I_o}{I_1}}\right) \tag{44}$$

This method of normalization ensures that fluctuations in the output intensity of the laser will not interfere with pressure measurements.

Most of the data were obtained from a system that used the 1-5/8-in.-diameter Monokote membrane or the 1-in. pellicle transducer. In both cases, the percent-of-range errors were typically less than 1 percent. For both membranes, this error corresponds to a pressure resolution sensitivity of better than ± 0.01 psi.

In fact, it is believed that one of the major sources of error arose from fluctuations in the reference pressure transducer signal as read by the system voltmeter for small signal voltages. Triggering the voltmeter to record the reference pressure at low pressures occasionally caused a jump in the signal, which then influenced the voltage recorded by the voltmeter. However, when the reference pressure was monitored visually with a digital voltmeter and entered manually into the pressure calculation routine, pressure resolutions of ± 0.001 psig, typically, were obtained for both membranes. Thus, it was demonstrated that the intensity ratio system has good potential for being incorporated into an automated data acquisition system with high pressure-resolution capabilities.

4.3 GEOMETRIC MEASUREMENT SYSTEM

The reaction of the transducer membrane to a pressure differential was also tested by measuring the area of the image at the observation plane. The measurement was made with the Millipore® system (Fig. 8), which is essentially an image-analysis computer consisting of a vidicon camera, a TV monitor, and a contrast-mode controller. The experimental setup was basically the same as that used in the intensity measurement system. The Millipore system shown in Fig. 8 was used in addition to the photodetector system. This allowed simultaneous comparison of three different pressure measurement techniques: the piezoelectric transducer, the intensity system, and the area measurement system. The same laser, transducers, and operating parameters were used as before.

Data for the Millipore system were acquired automatically through an interface with the Tektronix 4051 computer. The computer program takes direct readings of the reference pressure, measures the image and reference beam intensities, and determines the area of the image. The pressures were then calculated for the last two cases and compared with the reference pressure.

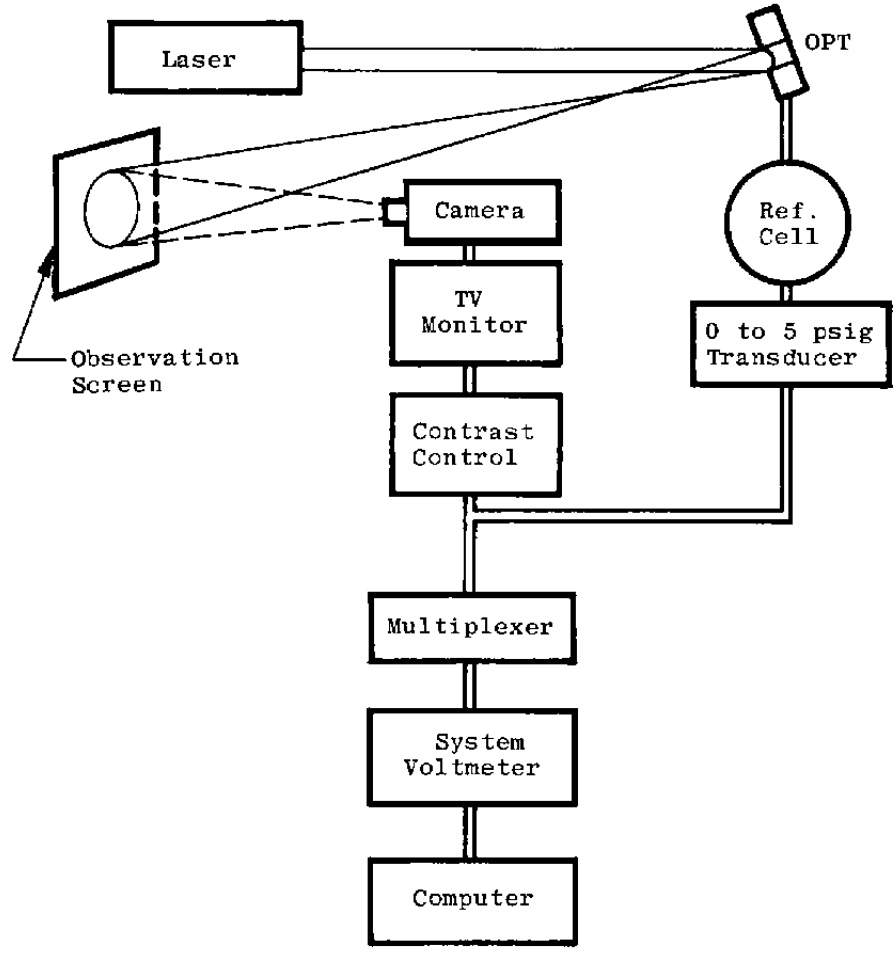

Figure 8. Geometric (Millipore®) System.

These measurements clearly parallel the expected behavior, shown by the theoretical curves (Fig. 7), with the normalized radius replaced by the square root of image area. The results obtained with the Millipore system compared quite well with those obtained with the intensity ratio method described earlier. As for the intensity system, the percent-of-range error for the Millipore system corresponded to pressure resolutions of about 0.01 psig.

A major source of error for the Millipore system was the contrast threshold adjustment. This function was controlled manually throughout data acquisition because it was necessary to readjust the contrast when the image size changed. However, this problem could be eliminated easily by using a more advanced image analysis system equipped with an automatic threshold monitor. Because of the nature of the geometric system, image aberrations could possibly occur. However, these mild distortions have little effect on accuracy.

5.0 LIMITATIONS

The application of optical membrane techniques is subject to unique constraints. Many of the constraints—such as meeting minimum spatial resolution requirements—do not differ significantly from those of conventional instrumentation systems. The most obvious limitation is the problem of optical access to the model and to the reflected image. Limitations also exist for conditions of turbulent environment, large unknown temperature variations, load-induced model deformation, and for various tracking requirements and particle impact effects.

5.1 TURBULENCE

Turbulence affects the OPT system in any one of several ways: through optical distortion and image degradation, by establishing a high-frequency response requirement, and by limiting the transducer size for boundary-layer studies.

With the exception of oblique passage through strong shocks, optical degradation is perhaps best analyzed experimentally. The optical index of refraction, n, can be related to the density of a gas through the Lorenz law

$$\frac{n^2 - 1}{n^2 - 2} = \rho_s K_{GD} \tag{45}$$

for gases, $n \approx 1$, and this reduces to the Gladstone-Dale law

$$n - 1 = \rho_s K_{GD}$$

where K_{GD} is the Gladstone-Dale constant. Together with a statistical model of the phase variations, this can yield information concerning beam distortions. The primary turbulence effects are beam deflection and scintillation.

Measuring pressure fluctuations in a turbulent boundary layer requires a high-frequency response that can be estimated. Previous work (Ref. 18) analyzed the power spectra of wall pressure fluctuations. The analysis correlated many data points at high frequencies for both supersonic and subsonic flows. The nondimensionalized frequency characterizing the high-frequency limit of the spectrum is given by

$$\frac{\omega \nu}{\bar{u}_T^2} = 0.056 \tag{46}$$

where ω is the vibrational frequency, ν is the kinematic viscosity, and $\bar{u}_T$ is the mean wall friction velocity

$$\bar{u}_T \equiv \sqrt{\frac{T_o}{\rho_o}} \tag{47}$$

where T_o is the mean wall shear stress and ρ_o the fluid density at the wall. For supersonic flow, the ratio $\bar{u}_T/u$ is approximately 0.03. From this the characteristic frequency is calculated:

$$f = \frac{\bar{\omega}}{2\pi} = \frac{0.0056}{2\pi} \frac{(0.03\ u_\infty)^2}{\nu}$$

for M = 1, f = 6 kHz. At the intermediate to high Mach numbers, this frequency quickly transcends the linear region of conventional transducers. A membrane transducer has an optimum response because of the low associated mass, resulting in a high frequency response.

Associated with the high-frequency response requirement in boundary-layer flow is a corresponding spatial resolution requirement. Experimentally verified values of the ratio of the rms pressure to free-stream dynamic pressure, $\sqrt{\bar{p}^2}/q_\infty$, show a steady linear decrease to a value of 0.5, the initial value for the nondimensionalized transducer radius range $0 < a < 50(\nu/\bar{u}_T)$. Beyond this value, the normalized pressure fluctuations remain relatively constant, exhibiting only a slight decrease with increased transducer radius. This represents an approximate upper limit for M = 1 and an aperture diameter of 2a = 0.0056 in. A transducer of such a small size would be difficult to fabricate; experience in OPT construction indicates the existence of a size constraint—a minimum radius of approximately 0.06 in.

5.2 TEMPERATURE DEPENDENCE

Another problem in the application of membrane transducers is the effect of temperature on membrane tension. Optical membranes must be designed that will respond to large temperature variations while retaining sensitivity to pressure.

Calibration of the membrane can minimize thermal effects when the uncertainty in temperature is small. In fact, even large temperature uncertainties may not appreciably affect the results. If the uncertainty in the effective tension due to temperature [Eq. (20)] is

small in comparison to the known portion of the tension, then temperature uncertainty effects are negligible (i.e., $\Delta T_{eff} << T_{eff}$, where ΔT_{eff} is the temperature-induced uncertainty effect). Thermal problems may also be reduced by the use of membrane materials with small thermal expansion coefficients, such as Invar®, or by simultaneous measurement of the transducer temperature.

Operation at high temperature (which, depending on the location of the transducer on a test article, could vary by several hundred degrees) is not necessarily a major problem because transducers could be constructed for most environmental conditions. However, lack of information about thermal variations could make the application of optical transducers difficult.

5.3 MODEL STRAIN

Surface strain caused by bending (e.g., wing flexure) may contribute significantly to the total error in a pressure measurement if the transducer touches the model material. Model surface deformation is an additional factor in the total strain of the membrane. The surface strain in a thin plate or bar is given by

$$\epsilon_s = \frac{\Delta \ell}{2\ell} = -\phi \frac{dr}{\ell}$$

where dr is the material thickness, ϕ is the angle of deflection, and ℓ is the undistorted length of the plate. This result holds for the concave side of a bar that is deformed to a circular arc segment with radius of curvature, R_c.

To estimate the magnitude of model strain, consider, for example, a model wing with a 12-in. span and a thickness of 0.5 in. For a deflection of 3 deg, the surface strain is on the order of 7×10^{-4}. An order of magnitude estimate for the thermal-induced strain on a Mylar membrane is about 10^{-5}. For the initial tension and the pressure-induced tension, the strains are both approximately 10^{-3}. Surface tension could reasonably be expected to cause an error of 10 percent in the pressure measurement. This error could be mathematically correctable if the deflection angle were known for each data point. A more practical solution, however, is to isolate the transducer mount from the test article with a layer of pliant material such as silicone rubber sealant, thus minimizing effects due to model surface strain.

5.4 IMAGE TRACKING

In the development of the pressure-radius relationship, paraxial illumination was assumed. Actual test situations will probably require off-axis illumination, which may produce additional optical aberrations and, thus, require geometric corrections to the shape of the image. Also, the projected image does not remain stationary during model attitude changes. For this reason, some type of image-tracking system will be required.

One feasible system investigated uses a set of scanning mirrors with a feedback mechanism for locking on to the target image. Angular calibration of the scanners as a function of input current allows the determination of the X- and Y-coordinates of the image on the observation plane. Suitable geometric corrections could then be applied. Other tracking systems, such as television or photographic image monitoring, could also be employed.

5.5 PARTICULATE IMPACTS

Pressure fluctuation caused by particle impacts is not significantly different from that encountered by conventional transducers. However, problems with membrane damage from impacts may occur with the electro-optical system. This problem would probably be more serious for plastic films than for metals.

Another universal limitation of electro-optical techniques is signal attenuation complicated by particles, vapor, and clouding of the optical components. Increasing the particle density in the atmosphere results in reduced visibility. Particulate matter can also contaminate the membrane surface, decreasing reflectivity. Generally these limitations do not exist for conventional transducers.

6.0 SUMMARY AND RECOMMENDATIONS

The current state of feasibility of the application of electro-optical surface pressure measurement techniques was evaluated and some of the advantages and limitations were identified. The results are summarized as follows:

1. The most promising method investigated involves using a reflective circular membrane. This technique functions by optical measurement of the deflection in the diaphragm caused by a uniform differential pressure loading. Optical determination of either the radius, area, or intensity of the projected image is used for measuring this deflection.

2. The electro-optical pressure measurement system proposed offers a complementary method to surface pressure determination. Optical membranes have been proven reliable and accurate in quasi-static situations. Resolutions as high as 0.001 psig, based on conventional transducer measurements, have been obtained in laboratory situations for 1-psi-range Mylar transducers and for a 0.2-psi-range nitrocellulose membrane. Through judicious choice of material properties, transducers of this type can be designed for optimum response and sensitivity in almost any pressure region.

3. The technology exists for fabricating relatively large transducers (greater than 1/8 in. in diameter) with suitable films of both plastics and metals. However, manufacturing technology does not yet exist for building the extremely small transducers required for high-frequency response or for cases requiring good spatial resolution.

4. Several potential problem areas have been identified. Most notable of these are effects caused by turbulence, temperature dependence, model strain, image geometry, and particulate impacts. To achieve high frequency response, small, clear apertures and extremely thin membranes are required. Present material properties and construction techniques may limit the application of the optical pressure transducer.

5. The possible applications for such a device are varied. Static pressures, in addition to high-frequency pressure variations, can be measured in both gases and liquids. Optical strain gages incorporating membranes of various shapes could be developed. For quasi-static (< 1 kHz) pressure measurements, the technique allows for simultaneous measurement of many points. This could be achieved by photographically recording, with a high-speed camera, the time history of spot diameters resulting from the overall illumination of a transducer pattern.

REFERENCES

1. Kastner, Marc and Forberg, R. R. "Pressure Dependence of Reflectivity of Se: Experimental Evidence for Large Local-Field Corrections." *Physical Review Letters*, Vol. 36, No. 13, 9 March 1976, pp. 740-744.

2. Theocaris, P. S., Philis, G. B., and Blontzou, C. H. "An Interferometric Method to Measure Transient Refractive Index, Birefringence and Thickness Variations of Solids." *Journal of Physics E: Scientific Instruments*, Vol. 8, July 1975, pp. 611-614.

3. Hayes, Hammond Vinton. "A New Reciever of Radiant Energy." *Review of Scientific Instrumentation*, Vol. 7, May 1936, pp. 202-204.

4. Zahl, Harold A. and Golay, Marcel J. E. "Pneumatic Heat Detector." *The Review of Scientific Instruments*, Vol. 17, No. 11, November 1946, pp. 511-515.

5. Golay, Marcel J. E. "A Pneumatic Infra-Red Detector." *The Review of Scientific Instruments*, Vol. 18, No. 5, May 1947, pp. 357-362.

6. Budal, K. "A New Microphone Based on an Optical Measuring Principle." *Journal of Sound and Vibration*, Vol. 36, No. 4, 1974, pp. 521-526.

7. Yellin, Martin. "Using Membrane Mirrors in Adaptive Optics." *Proceedings of the Society of Photo-Optical Instrumentation Engineers, Vol. 75, Imaging Through the Atmosphere*. Society of Photo-Optical Instrumentation Engineers, Palos Verdes Estates, California, 1976.

8. Grosso, R. P. and Yellin, M. "The Membrane Mirror as an Adaptive Optical Element." *Journal of the Optical Society of America*, Vol. 67, No. 3, March 1977, pp. 399-406.

9. Emmerling, R. "The Instantaneous Structure of the Wall Pressure Under a Turbulent Boundary Layer." Max-Planck-Institut fur Stroemungsforschung, Bench No. 9, 1973.

10. Emmerling, R., Meier, G. E. A., and Dinkelacker, A. "Investigation of the Instantaneous Structure of the Wall Pressure Under a Turbulent Boundary Layer Flow." *AGARD Conference Proceedings*, No. 131, Paris 1973, Paper 24.

11. Dinkelacker, A., Hessel, M., Meier, G. E. A., and Schewe, G. "Investigation of Pressure Fluctuations Beneath a Turbulent Boundary Layer by Means of an Optical Method." *The Physics of Fluids*, Vol. 20, No. 10, Part 2, October 1977, pp. 5216-5224.

12. Hetényi, Miklós Imre. *Handbook of Experimental Stress Analysis*. John Wiley and Sons, Inc., New York, 1957.

13. Bomar, B. W., Goethert, W. H., Belz, R. A., and Bentley, H. T., III. "The Development of a Displacement Interferometer for Model Deflection Measurements." AEDC-TR-76-116 (AD-A034384), January 1977.

14. Goethert, W. H. "Development and Application of a Laser Interferometer for Measurements of High Temperature Vibrating Surface." Master's Thesis. University of Tennessee, 1975.

15. Deferrari, Harry A. and Andrews, Frank A. "Laser Interferometric Technique for Measuring Small-Order Vibration Displacements." *The Journal of Acoustical Society of America*, Vol. 39, No. 5, Part 1, 1966, pp. 979-980.

16. Gaydon, A. G. and Hurle, I. R. *The Shock Tube in High-Temperature Chemical Physics*. Reinhold Publishing Corporation, New York, 1963.

17. Bolz, R. E. and Tuve, G. L., eds. *CRC Handbook of Tables for Applied Engineering Science*. Second edition. CRC Press, Cleveland, Ohio, 1977.

18. Black, Thomas J. "An Analytical Study of the Measured Wall Pressure Field under Supersonic Turbulent Boundary Layers." NASA CR-888, April 1968.

NOMENCLATURE

A	Surface area
a	Membrane radius
a_{mn}, b_{mn}, c_{mn}, d_{mn}	Constant coefficients
E	Modulus of elasticity
f	Focal length
f_c	Fringe constant
f_o	Fundamental frequency
I	Intensity
I_o	Initial beam intensity
I_p	Intensity at membrane surface
I_R	Reference intensity
J_{mn}	Spherical Bessel function
K_{GD}	Gladstone-Dale constant
ℓ	Undistorted length of the plate
M	Mach number
n	Fringe order
OPT	Optical pressure transducer
P	Pressure differential
P_B	Bursting pressure
P_o	Initial pressure
P_y	Yield pressure
R_c	Radius of curvature
r	Image radius/radial distance from optical axis
S	Sound level

T	Tension
T_{eff}	Effective tension
T_o	Initial tension
t	Time
Δt	Temperature difference
$\bar{u}_T$	Mean wall friction velocity
u_∞	Free-stream velocity
Y	Membrane displacement
Y_m	Maximum displacement
Z	Distance from transducer to observation plane
Z_f	Image distance
Z_s	Point source distance
α	Coefficient of thermal expansion
β	Damping factor
δ	Membrane thickness
ϵ	Linear strain (Cartesian coordinates)
ϵ_A	Area strain
ϵ_S	Surface strain caused by bending
ϵ_x, ϵ_y	Components of linear strain
θ	Membrane deflection angle
λ	Wavelength of light
μ	Poisson's ratio
ν	Kinematic viscosity

ξ	Axial distance from beam waist
ϱ	Illuminated aperture radius
ϱ_o	Fluid density at the wall
ϱ_s	Mass density
σ	Stress
σ_1, σ_2	Principle stressses
$\sigma_x, \sigma_y, \sigma_z$	Stress components
σ_N	Ultimate strength
σ_s	Yield strength
τ_o	Mean wall shear stress
ϕ	Model strain deflection angle
ψ	Linear function of image radius (defined in text)
Ω	Beam waist
Ω_o	Beam waist radius at $1/e^2$ point
ω	Vibrational frequency
ω_o	Fundamental frequency